Centrum voor Wiskunde en Informatica

REPORT*RAPPORT*

MAS

Modelling, Analysis and Simulation

Modelling, Analysis and Simulation

Simulation techniques for the population dynamics of sinking phytoplankton in light-limited environments

J. Huisman, B.P. Sommeijer

REPORT MAS-R0201 JANUARY 31, 2002

CWI is the National Research Institute for Mathematics and Computer Science. It is sponsored by the Netherlands Organization for Scientific Research (NWO).
CWI is a founding member of ERCIM, the European Research Consortium for Informatics and Mathematics.

CWI's research has a theme-oriented structure and is grouped into four clusters. Listed below are the names of the clusters and in parentheses their acronyms.

Probability, Networks and Algorithms (PNA)

Software Engineering (SEN)

Modelling, Analysis and Simulation (MAS)

Information Systems (INS)

P.O. Box 94079, 1090 GB Amsterdam (NL)
Kruislaan 413, 1098 SJ Amsterdam (NL)
Telephone +31 20 592 9333
Telefax +31 20 592 4199

ISSN 1386-3703

Simulation Techniques for the Population Dynamics of Sinking Phytoplankton in Light-Limited Environments *

Jef Huisman †
Aquatic Microbiology, Institute for Biodiversity and Ecosystem Dynamics
University of Amsterdam
Nieuwe Achtergracht 127, 1018 WS Amsterdam, The Netherlands
jef.huisman@chem.uva.nl

Ben Sommeijer
CWI
P.O. Box 94079, 1090 GB Amsterdam, The Netherlands
bsom@cwi.nl

ABSTRACT
Phytoplankton use light for photosynthesis, and the light flux decreases with depth. As a result of this simple light-dependence, reaction-advection-diffusion models describing the dynamics of phytoplankton species contain an integral over depth. That is, models that simulate phytoplankton dynamics in relation to mixing processes generally have the form of an integro-partial differential equation (integro-PDE). Integro-PDEs are computationally more demanding than standard PDEs. Here, we outline a reliable and efficient technique for numerical simulation of integro-PDEs. The simulation technique is illustrated with several examples on the population dynamics of sinking phytoplankton, a species group that is most relevant in the context of the global carbon cycle. Our results confirm recent findings that Sverdrup's critical-depth theory breaks down if turbulent mixing is reduced below a critical turbulence. We therefore conclude that models that do not carefully consider the population dynamics of phytoplankton in relation to the turbulence structure of the water column may easily lead to erroneous predictions.

2000 Mathematics Subject Classification: 92D25, 65M20.
1998 ACM Computing Classification System: I.6.5, J.3, G.1.7 and G.1.8.
Keywords and Phrases: Phytoplankton, Stratification, Competition, Numerical modelling, Integro-partial differential equation.
Note: Work carried out under subtheme MAS1.1 - Applications from the Life Sciences.

*The investigations were supported by the Earth and Life Sciences Foundation (ALW), which is subsidized by the Netherlands Organization for Scientific Research (NWO).
†Correspondence and requests for materials should be addressed to the first author.

1 Introduction

By means of their photosynthetic carbon fixation, phytoplankton extract carbon from the atmosphere, and part of this carbon ultimately sinks into the ocean interior. As a result, primary production by marine phytoplankton plays an important role in the global carbon cycle [12, 1, 42]. The factors determining the production of marine phytoplankton are gradually becoming better understood [27, 13, 25]. In some oceanographic regions, and some seasons, phytoplankton growth is primarily limited by the availability of nutrients like iron, nitrogen, and phosphorus [28, 31, 2, 4]. In other oceanographic regions, and other seasons, light availability and light-nutrient interactions are major factors limiting phytoplankton production [29, 34, 37, 23]. Light limitation is thought to be particularly relevant in upwelling regions where nutrients are in ample supply, in turbid waters, and also in nutrient-poor environments when during periods of turbulent weather phytoplankton are exposed to the low light conditions encountered during deep mixing. In this paper, we will discuss the dynamics of sinking phytoplankton species in such light-limited environments.

Recent theory [22, 26, 20], experiments [32, 39, 40], and field observations [6, 3, 36, 24] show that the turbulence structure of the water column can have a major impact on the population dynamics of phytoplankton species in light-limited environments. In particular, theory developed by Huisman et al. [20, 21, 18] and Ebert et al. [11] shows that the dynamics and species composition of phytoplankton communities may change drastically if the turbulent mixing rate is reduced below a critical threshold value. Models that lack information on the turbulence structure of the water column might therefore seriously misjudge opportunities for phytoplankton bloom development.

Mathematical tools are available to model phytoplankton dynamics in relation to turbulent mixing and transport processes, borrowing techniques from computational fluid dynamics [34, 35, 10, 26]. These models are often cast in terms of partial differential equations (PDEs) of the reaction-advection-diffusion type. A common problem with numerical simulation of PDEs is that their spatial and temporal discretization may lead to numerical artifacts [16, 14]. For instance, a coarse discretization, or a discretization using inadequate formulas for transport phenomena, may easily lead to wiggles in the spatial domain that amplify in time to yield completely unrealistic solutions. These problems can be diminished by increasing the spatial and temporal resolution, but this of course results in very time-consuming simulations. This particularly applies to phytoplankton models, which contain a highly nonlinear reaction term representing light-dependent primary production. The reaction term appears in the model as an integral over depth, because primary production at a certain depth depends on the light intensity at that depth, which in turn depends on light absorption by all phytoplankton cells above that depth. Owing to this depth integral, the PDE model can be classified as an integro-PDE. Simulation of integro-PDEs is computationally more demanding than simulation of standard PDEs, and therefore requires an efficient numerical approach.

The aim of this paper is to outline an efficient numerical technique for simulation of phytoplankton dynamics in light-limited environments. The approach is illustrated with several examples.

2 The model

The mathematical structure of our model is based on Huisman et al. [20, 21, 18] and Ebert et al. [11]. We consider a water column with a cross section of one unit area. Let z denote the depth coordinate within the water column, where z runs from 0 at the top to a maximum depth, z_m, at the bottom. Let $I(z,t)$ denote the light intensity at depth z and time t, and let $\omega(z,t)$ denote the phytoplankton population density (cells per unit volume) at depth z and time t.

Light gradient: Photons are absorbed by water, clay particles, phytoplankton species, and many other light-absorbing substances. We assume that the light gradient follows Lambert-Beer's law, which states that light absorption at depth z is proportional to the concentration of light absorbers at this depth:

$$\frac{\partial I}{\partial z}(z,t) = -\left(k\,\omega(z,t) + K_{bg}\right) I(z,t), \tag{1}$$

where k is the specific light attenuation coefficient of the phytoplankton, and K_{bg} is the background turbidity owing to light absorption by all non-phytoplankton components in the water column. Integrating this equation over depth gives the following light intensity at depth z and time t:

$$I(z,t) = I_{in}\; e^{-K_{bg} z}\; e^{-k \int_0^z \omega(\sigma,t)\, d\sigma}, \tag{2}$$

where I_{in} is the incident light intensity, and σ is an integration variable. We note that this formulation includes light absorption by phytoplankton. Thus, the light gradient changes with a change in the phytoplankton population density distribution.

Population dynamics: The changes in the phytoplankton population density distribution can be described by the partial differential equation

$$\frac{\partial \omega}{\partial t}(z,t) = g(I(z,t))\,\omega(z,t) - \frac{\partial J}{\partial z}(z,t). \tag{3}$$

Here $g(I(z,t))$ is the specific growth rate of phytoplankton as a function of the light intensity $I(z,t)$, and $J(z,t)$ is the vertical flux of phytoplankton at depth z and time t. The minus sign indicates that an increase of the flux with depth has a negative effect on the local population density.

The specific growth rate in (3) depends on the balance between production and losses:

$$g(I) = p(I) - \ell, \tag{4}$$

where $p(I)$ is the specific production rate as a function of light intensity, and ℓ is the specific loss rate. We used a simple rational function for $p(I)$ (cf. [30, 19]):

$$p(I) = \frac{p_{max} I}{H + I}, \tag{5}$$

where p_{max} is the maximal specific production rate and H is a half-saturation constant.

The vertical flux of phytoplankton in (3) depends on the sinking rate of phytoplankton and on transport of phytoplankton by turbulent diffusion:

$$J(z,t) = v\,\omega(z,t) - D(z)\,\frac{\partial \omega}{\partial z}(z,t), \tag{6}$$

where v is the vertical velocity of the phytoplankton, and $D(z)$ is the turbulent diffusion coefficient at depth z. The positive sign of the first term on the right-hand side of (6) implies that $v > 0$ for sinking phytoplankton. The minus sign in the second term on the right-hand side indicates that turbulent diffusion is in the direction opposite to the concentration gradient.

We assume that the boundaries of the system are closed:

$$J(0,t) = v\,\omega(0,t) - D(0)\,\frac{\partial \omega}{\partial z}(0,t) = 0, \tag{7a}$$

and

$$J(z_m,t) = v\,\omega(z_m,t) - D(z_m)\,\frac{\partial \omega}{\partial z}(z_m,t) = 0. \tag{7b}$$

Thus, phytoplankton cannot leave the water column, neither at the top nor at the bottom.

Substituting (2), (4) and (6) into (3) yields our key equation for the population dynamics:

$$\frac{\partial \omega}{\partial t} = p(I_{in}\,e^{-K_{bg}z}\,e^{-k\int_0^z \omega(\sigma,t)d\sigma})\,\omega - \ell\,\omega - v\,\frac{\partial \omega}{\partial z} + \frac{\partial}{\partial z}\left(D(z)\,\frac{\partial \omega}{\partial z}\right). \tag{8}$$

Formally, this is an integro-partial differential equation. The integral within the first term on the right-hand side of the equation is a non-local term, which indicates that the light intensity at a certain depth z depends on all population densities above depth z.

3 Simulation technique

To obtain a fully discrete solution in space and time we will follow the so-called Method of Lines (MOL) approach. That is, first the spatial differential operators as well as the integral term will be replaced by discrete approximations and subsequently the resulting system of ordinary differential equations (ODEs), which is still continuous in time, will be integrated numerically.

3.1 Spatial discretization

First, we define a spatial grid on the interval $0 \le z \le z_m$. In case a priori knowledge about the solution is available, the grid can be chosen with relatively many points in regions where a high spatial activity is expected. In fact, the software that we developed indeed offers this facility. However, to avoid unnecessary complications in the description, the numerical procedure will here be explained on the basis of an equidistant grid and with a uniform turbulent diffusion coefficient.

Hence, let us define our spatial grid by:

$$s_0 = 0, \quad s_i = (i - \tfrac{1}{2})\Delta z, \quad i = 1, ..., N, \quad s_{N+1} = z_m, \tag{9}$$

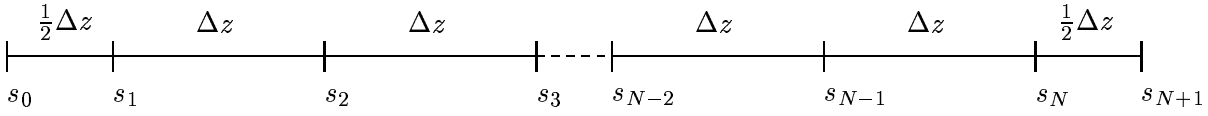

where $\Delta z := z_m/N$. Furthermore, by $w_i(t)$, $i = 1, ..., N$, we denote an approximation to $\omega(s_i, t)$. To discretize the derivative of the flux (i.e., the term $\partial J(z,t)/\partial z$ in (3)) in the point s_i, we will use a finite volume approach. That is, we assume an imaginary box around the point s_i, at the boundaries of which we approximate the fluxes, using the numerical values w_i at the grid points.

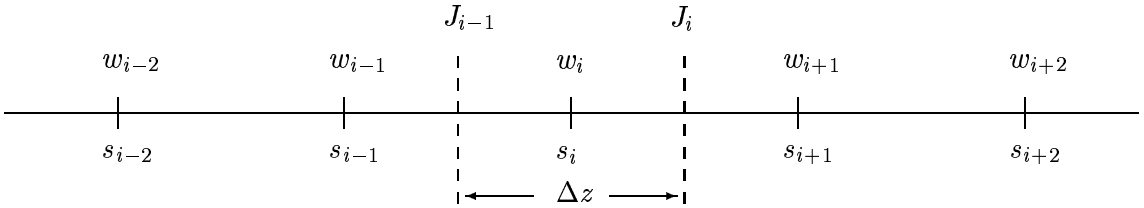

In this way we obtain *conservation* of the quantity J since the numerical approximation that we use for a particular flux $J_i \approx J(s_i + \frac{1}{2}\Delta z, t)$ serves as outflow for one particular box and at the same time as inflow for the adjacent box. Now, $\partial J(z,t)/\partial z$ in the point $z = s_i$ is approximated by $(J_i - J_{i-1})/\Delta z$. Next, we need an approximation for J_i. Here we use the approach that is nowadays standard in the field of Computational Fluid Dynamics for the numerical solution of advection-diffusion equations. That is, the diffusion term is discretized symmetrically, whereas for the advection term a third-order, so-called *upwind* discretization is used (see e.g., [16]). To be more precise, in case of sinking, where the flow is from left to right in the above figure, we use (cf. (6))

$$\begin{aligned} J_i &= v\,\omega(s_i + \tfrac{1}{2}\Delta z, t) - D\,\frac{\partial \omega}{\partial z}(s_i + \tfrac{1}{2}\Delta z, t) \\ &\approx v\,\tfrac{1}{6}\,[-w_{i-1} + 5w_i + 2w_{i+1}] - D\,\frac{w_{i+1} - w_i}{\Delta z}. \end{aligned} \tag{10}$$

This expression explains the term 'upwind': we see that more information from the left (i.e., the upstream region in case of sinking) has been used. Analogously, in case of buoyant phytoplankton, we might again use a third-order upwind discretization, now using more information from the right, resulting in the approximation

$$J_i \approx v\,\tfrac{1}{6}\,[2w_i + 5w_{i+1} - w_{i+2}] - D\,\frac{w_{i+1} - w_i}{\Delta z}. \tag{11}$$

We remark that a symmetric discretization of the advection term easily leads to 'wiggles' in the numerical solution. By this we mean that, in the neighborhood of a drastic change

in the solution, undershoot and overshoot values will develop. Especially in case of undershoot (i.e., too low values) this may lead to negative solution components. A negative population density is of course not realistic. The use of upwind techniques drastically reduces this unwanted property.

The fluxes J_0 and J_N vanish according to the boundary conditions, and for J_1 we use a symmetric formula since we lack sufficient upstream information (in case of sinking).

Summarizing, for sinking phytoplankton, we arrive at the following set of ODEs:

$$\frac{dw_i(t)}{dt} = g_i\, w_i - \frac{J_i - J_{i-1}}{\Delta z}, \quad i = 1, ..., N, \tag{12}$$

where

$$\begin{aligned} J_0 &= 0, \\ J_1 &= v\, \frac{w_2 + w_1}{2} - D\, \frac{w_2 - w_1}{\Delta z}, \\ J_i &= v\, \tfrac{1}{6}[-w_{i-1} + 5w_i + 2w_{i+1}] - D\, \frac{w_{i+1} - w_i}{\Delta z}, \quad i = 2, ..., N-1, \\ J_N &= 0. \end{aligned} \tag{13}$$

The term g_i in (12) is defined as $g_i := p(I_i) - \ell$, where I_i denotes the light intensity at $z = s_i$. Replacing the integral term by the repeated trapezoidal rule, the light intensity is approximated by

$$I_i = I_{in}\, e^{-K_{bg} s_i}\, e^{-k[\frac{1}{4}w_0 + \frac{3}{4}w_1 + w_2 + ... + w_{i-1} + \frac{1}{2}w_i]\Delta z}, \tag{14}$$

with the solution at the surface, w_0, extrapolated from inside: $w_0 = (3w_1 - w_2)/2$.

3.2 Time integration

After spatial discretization we arrive at a large system of ODEs, written in the form

$$\frac{d\mathbf{w}(t)}{dt} = \mathbf{F}(\mathbf{w}(t)), \quad t \geq 0, \tag{15}$$

where the vector $\mathbf{w}(t) \in \mathbb{R}^N$ contains the components $w_i(t)$. Our first observation is that this system is a *stiff* ODE. This means that the Jacobian matrix $\partial\mathbf{F}/\partial\mathbf{w}$ has widely spread eigenvalues (for a discussion on stiffness we refer to [15]). To handle the stiffness of the ODE system, we selected an *implicit* integration method, which has, in general, adequate stability properties to treat the stiff system. As a consequence, however, we are now faced with the task to solve, in each time step, a system of implicit relations to obtain the solution at the next point in time. For the family of implicit methods that we have used, this results in solving the equation

$$\mathbf{R}(\mathbf{W}_{n+1}) := \mathbf{W}_{n+1} - b_0\, \Delta t\, \mathbf{F}(\mathbf{W}_{n+1}) - \sum_{i=1}^{m} b_i\, \mathbf{W}_{n+1-i} = \mathbf{0}. \tag{16}$$

Here, $\mathbf{W}_{n+1}$ is an approximation to $\mathbf{w}(t)$ at $t = t_{n+1} := (n+1)\Delta t$, Δt being the time step, and the coefficients b_i are defined by the method in use. $\mathbf{W}_n, \mathbf{W}_{n-1}, ..., \mathbf{W}_{n+1-m}$ are approximate solutions at previous points in time and serve to give the method the required accuracy.

As usual, (16) is iteratively solved by means of Newton's process. That is, a series of linear systems of the form

$$[I - b_0\ \Delta t\ \partial\mathbf{F}/\partial\mathbf{w}] \left[\mathbf{W}_{n+1}^{j} - \mathbf{W}_{n+1}^{j-1}\right] = -\mathbf{R}(\mathbf{W}_{n+1}^{j-1}),\ \ j = 0, 1, ..., \tag{17}$$

have to be solved, where I denoted the identity matrix. The iterates $\mathbf{W}_{n+1}^{j}$ hopefully converge to the solution $\mathbf{W}_{n+1}$.

The Jacobian matrix $\partial\mathbf{F}/\partial\mathbf{w}$ is composed of a 4-diagonal band (originating from the discretization of the advection-diffusion terms) plus a lower triangular part (due to the integral term). This makes the solution of the linear systems in (17) in the Newton process very time-consuming. To improve the numerical efficiency, we neglected the lower triangular part in the Jacobian matrix. This still yields the required convergence, but results in a larger number of iterations. In fact, the total number of Newton iterations (summed over all steps) increased by 30-50%, but this is amply compensated by the strongly reduced costs to solve the linear systems (which now have a simple band structure).

Brown et al. [5] implemented the above numerical time integration technique in their code VODE, which we have used to produce the results described in the present paper. This code belongs to the family of most widely used stiff ODE solvers and is freely available from http://www.netlib.org/ode/ (both in Fortran and C). VODE is very robust in the sense that it includes all kind of strategies, necessary for automatic integration and incorporates experience of many users over a long period.

4 Applications

4.1 Unstratified waters

Model structure: In the spirit of Ockham's razor ('*Essentia non sunt multiplicanda*'), we first consider one of the simplest scenarios. We assume that the water column is unstratified, with a uniform turbulent diffusion coefficient $D(z) = D$ (see Fig. 1A). The depth of the water column is 100 m, divided in an equidistant grid of 1000 cells.

Results: Figure 2 illustrates the time course of the population density distribution of a sinking species in such an unstratified water column. The parameter values used in this simulation are specified in Table 1. The simulation starts with a uniform population density distribution (Fig. 2A). Part of the population sinks to the bottom and vanishes in the dark (Fig. 2B,C). Ample light conditions in the upper part of the water column, however, allow the growth rate to overcome both the sinking and mixing rates. As a result, a phytoplankton bloom develops in the upper 30 meters of the water column (Fig. 2D-F).

The simulations were repeated for a wide variety of different water-column depths and turbulent diffusion coefficients. For each simulation we monitored whether the sinking species was capable to sustain a population or whether the population *as a whole* vanished

Table 1: Variables and parameter values used in the simulations.

Symbol	Meaning	Value	Units
Variables			
I	light intensity		μmol photons $\cdot m^{-2} \cdot s^{-1}$
ω	population density		cells $\cdot m^{-3}$
Parameters			
D	turbulent diffusion	5	$cm^2 \cdot s^{-1}$
H	half-saturation constant of light-limited growth	30	μmol photons $\cdot m^{-2} \cdot s^{-1}$
I_{in}	incident light intensity	350	μmol photons $\cdot m^{-2} \cdot s^{-1}$
K_{bg}	background turbidity	0.2	m^{-1}
k	specific light attenuation of phytoplankton	$15 \cdot 10^{-12}$	$m^2 \cdot$ cell^{-1}
ℓ	specific loss rate	0.01	h^{-1}
p_{max}	maximal specific production rate	0.04	h^{-1}
v	vertical velocity	0.04	$m \cdot h^{-1}$
z_m	water column depth	100	m
z_T	thermocline depth*)	20	m

*) Note: only in stratified waters.

in the dark. Following Huisman et al. [20], we say that there is 'bloom development' whenever a population can be sustained. The results of this exercise are shown in Fig. 3. This reveals that the conditions for bloom development of sinking phytoplankton species in unstratified waters can be summarized as follows [11, 18]:

- If turbulence is high, the phytoplankton population is uniformly mixed. In this case, if the water column depth exceeds a critical depth (sensu Sverdrup [38]), depth-averaged light conditions experienced by the phytoplankton become too low to allow net phytoplankton growth.

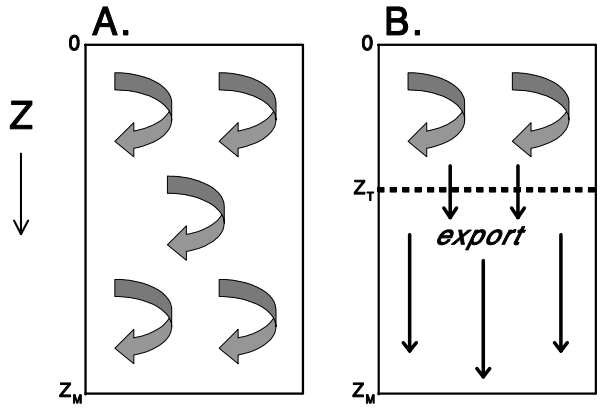

Figure 1: Model structure. (A) Unstratified water column. (B) Stratified water column.

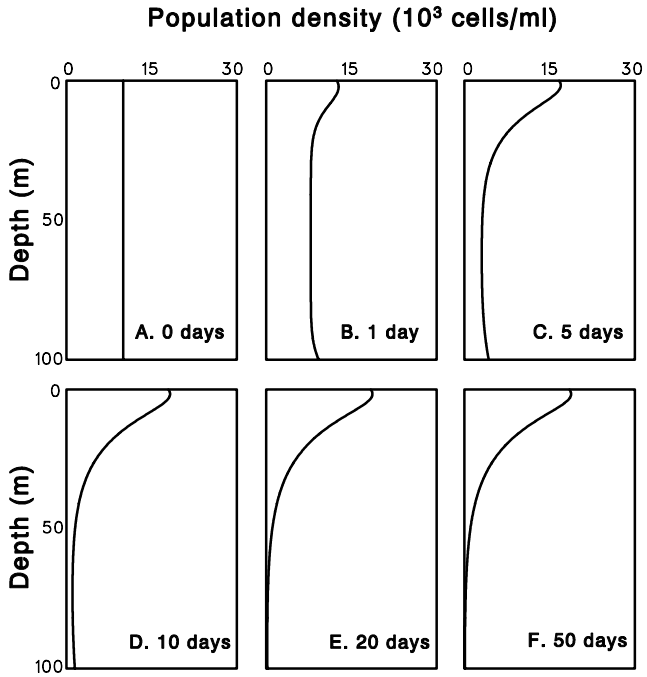

Figure 2: Time course of phytoplankton bloom development in an unstratified water column. Parameter values: see Table 1.

- If turbulent diffusion remains between a maximal turbulence and a minimal turbulence, the phytoplankton population can outgrow both mixing rates and sinking rates, and hence the population can be sustained even in deep waters. We note that the maximal turbulence is conceptually equivalent to the critical turbulence described by Huisman et al. [20] and that the minimal turbulence can be traced back to Riley et al. [33, p. 90].

- If turbulence is low, then there is no force that prevents sinking of the entire phytoplankton population to the bottom of the water column. In this case, if the depth of the water column exceeds the compensation depth, the population vanishes in the dark.

4.2 Stratified waters

Model structure: Suppose that the water column is stratified into two layers, separated by a thermocline (Fig. 1B). The depth z_T indicates the position of the thermocline. We here assume that only the upper mixed layer is subject to turbulent mixing, whereas vertical turbulence is negligible in the deeper water. Accordingly, we set $D(z) = D$ above the thermocline and we set $D(z) = 0$ below the thermocline. Assuming continuity of the flux, the flux of phytoplankton at the thermocline equals

$$J(z_T, t) = v\,\omega(z_T, t). \tag{18}$$

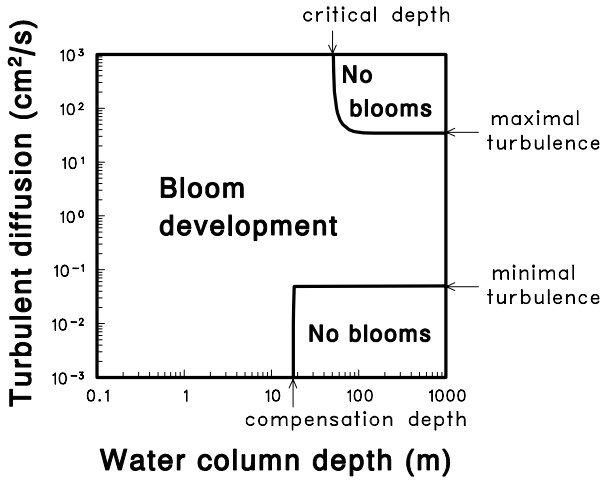

Figure 3: Combinations of water-column depth, z_m, and turbulent diffusion coefficient, D, that allow bloom development of sinking phytoplankton species in unstratified waters. The graph is based on a grid of 41 x 61 = 2,501 simulations. Parameter values: see Table 1.

This boundary condition replaces the boundary condition in (7b). We note that a boundary condition at the bottom of the water column (i.e., at $z = z_m$) is no longer necessary, since the assumption $D(z) = 0$ below the thermocline simplifies (8) to a first-order PDE with respect to z in the deep water layer.

Numerical simulation: This stratified model structure has several implications for the spatial discretization. We model the fluxes above the thermocline as defined in (13), with the exception that $J_N = 0$ is replaced by $J_N = v\,[3w_N - w_{N-1}]/2$. Hence, the solution at the thermocline is extrapolated from above. In this way the flux through the thermocline is only influenced by the solution above this point, which is of course realistic in case of sinking phytoplankton.

The N cells in the upper water layer are supplemented by a grid of M cells in the deep water layer. The grid in the deep water layer is essentially similar to the grid described in (9), but now $s_{N+i} = z_T + (i - \frac{1}{2})\Delta z$, where $i = 1, ..., M$ and $\Delta z = (z_m - z_T)/M$. For the influx at the thermocline, we use the 'extrapolated' expression J_N given above to assure continuity of the flux. All fluxes below the thermocline are simulated by

$$J_{N+i} = v\; w_{N+i}, \quad i = 1, ..., M. \tag{19}$$

Notice that this is again an upwind approximation. The difference with the expression in (10), apart from zero diffusion, is that here the advection term is only first-order accurate, whereas (10) is based on a third-order approximation. The reason for changing to first-order is that the first-order discretization has better properties to keep the solution positive. Since the solution is usually close to zero in the deeper part of the water column, this feature is considered of more importance than the drop in order of accuracy. The reaction term g_i is treated similarly as in the case of unstratified waters.

Results: The time course of the population density distribution in a stratified water

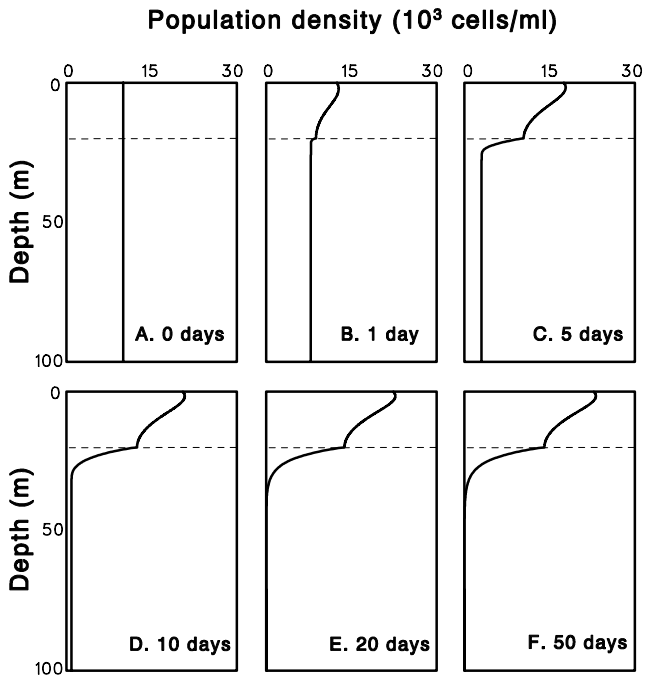

Figure 4: Time course of phytoplankton bloom development in a stratified water column. The horizontal dashed line indicates the depth of the thermocline. Parameter values: see Table 1.

column is shown in Fig. 4, using the same species as in Fig. 2. Again, the simulation starts with a uniform population density distribution (Fig. 4A). Owing to sinking and mortality, population densities in the lower water layer decrease in time (Fig. 4B-D). In contrast, the ample light conditions in the upper mixed layer sustain a phytoplankton population. In this particular example, the upper mixed layer is not sufficiently turbulent to homogenize the population density distribution throughout the upper mixed layer, and hence a conspicuous depth profile develops (Fig. 4B-D). Part of the population in the upper mixed layer sinks over the thermocline. As a result, the population density distribution below the thermocline decays nearly exponentially with depth (Fig. 4D-F).

Again the simulations were repeated for a wide variety of different thermocline depths and turbulent diffusion coefficients. This yields Fig. 5. Accordingly, the conditions for bloom development of sinking phytoplankton species in stratified waters can be summarized as follows:

- If the thermocline is too shallow, the flux of sinking phytoplankton over the thermocline exceeds the depth-integrated growth rate in the upper mixed layer. Hence, below a minimal thermocline depth, the phytoplankton population cannot be sustained.

- If turbulent mixing is intense and the thermocline exceeds a maximal depth, depth-averaged light conditions in the upper mixed layer become too low to allow net phytoplankton growth. We note that the maximal depth in Fig. 5 is slightly shallower than the critical depth (sensu Sverdrup [38]) in Fig. 3.

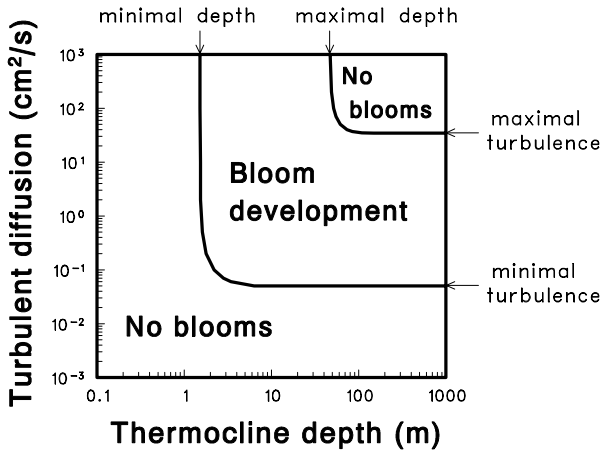

Figure 5: Combinations of thermocline depth, z_T, and turbulent diffusion coefficient, D, that allow bloom development of sinking phytoplankton species in stratified waters. The graph is based on a grid of 41 x 61 = 2,501 simulations. Parameter values: see Table 1.

- If turbulent diffusion remains between a maximal turbulence (cf. Huisman et al. [20]) and a minimal turbulence (cf. Riley et al. [33]), then the phytoplankton population can outgrow both mixing rates and sinking rates. The maximal and minimal turbulence in Fig. 5 have the same values as in Fig. 3.
- If turbulence is too low, the phytoplankton population is lost from the upper mixed layer and vanishes into the dark.

4.3 Competition

Model structure: Most waters are inhabited by a multitude of phytoplankton species. Therefore, this section considers competition between a number of n species. The different species are indicated by subscripts such as i and j. We assume that there is no direct interference between the species. The species interact only indirectly, through shading. Hence, our multispecies version of the model is a straightforward extension of the single-species model:

$$\frac{\partial \omega_i}{\partial t} = p_i(I(z,t))\,\omega_i - \ell_i\,\omega_i - v_i\,\frac{\partial \omega_i}{\partial z} + \frac{\partial}{\partial z}\left(D(z)\,\frac{\partial \omega_i}{\partial z}\right), \quad i = 1, ..., n, \tag{20}$$

where the vertical light gradient is given by

$$I(z,t) = I_{in}\; e^{-K_{bg} z}\; e^{-\int_0^z \left(\sum_{j=1}^n k_j\,\omega_j(\sigma,t)\right) d\sigma}. \tag{21}$$

Numerical simulation: Here, the spatial discretization is similar as in the single-species case. However, since the dimension of the system of ODEs in (15) is now n times as large, the true Jacobian matrix in the Newton process (including the lower triangular parts due to the discretized integral term) has a huge number of entries. Hence, especially in this situation, it is recommendable to use a simplified Jacobian matrix that neglects the lower

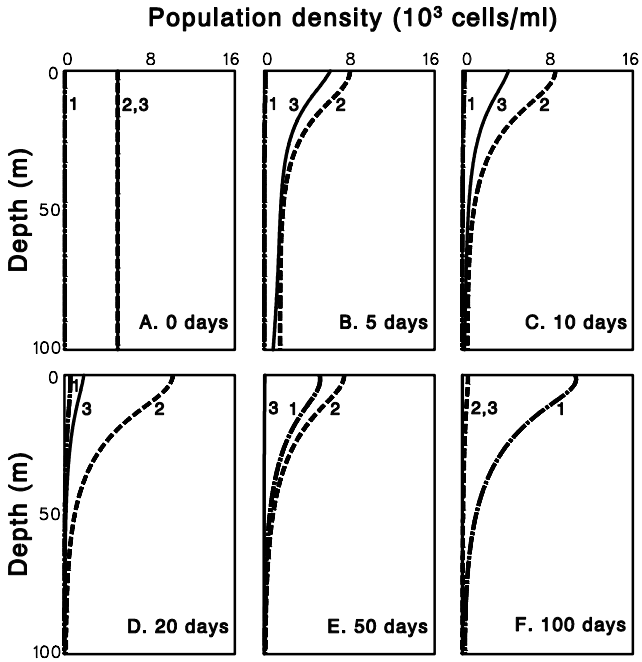

Figure 6: Time course of competition for light between a sinking phytoplankton species (species 1), a neutrally buoyant phytoplankton species (species 2), and a buoyant phytoplankton species (species 3) in an unstratified water column. In the end, the sinking species wins. Environmental parameters as in Table 1, except $D = 10\, cm^2 \cdot s^{-1}$ Species parameters: see Table 2.

triangular parts originating from the integral term and consists only of the four diagonals. In this way, a dramatic reduction in the computational costs for solving the linear systems in (17) can be obtained without sacrificing the rate of convergence of the Newton process too drastically.

Results: As an illustration, we consider three phytoplankton species: a sinking species, a neutrally buoyant species, and a buoyant species. All three species have rather similar growth characteristics, except that the sinking species has a higher maximal specific production rate than the neutral species, which in turn has a higher maximal specific production rate than the buoyant species (see Table 2). Our simulation experiment considers a relatively turbulent, unstratified water column with a depth of 100 m. All three species are uniformly distributed over depth at the onset of the simulation experiment. The neutral species and buoyant species are both given an initial advantage; at the onset of the experiment they are 100 times more abundant than the sinking species (Fig. 6A). During the first few days, both the buoyant and neutral species increase in the upper part of the water column, and decrease in the deeper parts (Fig. 6B). Because turbulent mixing is quite intense, however, the buoyant species remains vertically dispersed over the upper 50 meters, and is therefore unable to form a surface bloom. Owing to the increased population densities in the upper part of the water column, the light gradient becomes steeper. As a result, the buoyant species starts to decline and the neutral species gains dominance

Table 2: Species parameters used in Fig. 6.

Parameter	Sinking species (species 1)	Neutral species (species 2)	Buoyant species (species 3)	Units
v_i	$+4.2$	0	-8.3	$cm \cdot h^{-1}$
$p_{max,i}$	0.04	0.03	0.02	h^{-1}
H_i	10	10	20	μmol photons $\cdot m^{-2} \cdot s^{-1}$
ℓ_i	0.01	0.01	0.01	h^{-1}
k_i	0.30	0.15	0.15	$cm^2 \cdot$ (million cells)$^{-1}$
$\omega_i(z,0)$	50	5000	5000	cells $\cdot cm^{-3}$

Note: Parameter values were all chosen within the typical range measured for freshwater phytoplankton species from the culture collection of the Laboratory of Aquatic Microbiology, University of Amsterdam, The Netherlands (e.g. [40, 41, 8, 17, 19]).

(Fig. 6C). At the same time, however, the sinking species increases (Fig. 6D), because the high turbulent mixing rate prevents its sedimentation and because its high specific growth rate allows proliferation under rather low light conditions. The sinking species eventually displaces the neutral species (Fig. 6E), and becomes dominant (Fig. 6F).

5 Discussion

This discussion will focus on the numerical technique and on the biological interpretation of our findings.

Numerical simulation of PDEs generally consists of two steps: spatial discretization of the PDE and subsequent time integration of the resulting ODE system. The simplest spatial discretization of a PDE would be based on symmetrical discretization of the advection and diffusion terms. In preliminary simulations (not shown) we observed, however, that a completely symmetrical discretization of plankton PDEs easily leads to numerical artifacts in the form of expanding spatial oscillations ('wiggles'). The results presented here show that such spatial instabilities are effectively removed by introducing upwind methods for spatial discretization of the advection terms.

The simplest time integration of the resulting ODE system would be based on an explicit time integration method. However, explicit time integration failed owing to the stiffness of our ODE problem. That is, an explicit method, which is simple and computationally cheap per time step, would be forced by the stiff system to take very small time steps in order to avoid numerical instabilities. This time step restriction is so severe in our application that it is unfeasible to use an explicit integration method. Therefore, we selected an implicit method. However, owing to the depth integral in our phytoplankton model, the implicit method is computationally very demanding because the Jacobian matrix in the iterative scheme has a non-zero lower triangular part. This problem was tackled by simply neglecting the lower triangular part of the Jacobian matrix. We mention that the depth integral is of course taken into account in the model itself (in the g_i term); it is neglected only in the Jacobian matrix of the iterative scheme used to solve the implicit relation. This simplification still yields the required convergence, though after a larger

number of iterations. The increased number of iterations is clearly offset by a much faster handling of the simplified Jacobian matrix. A simplified Jacobian matrix is particularly useful in the context of competition between species, since the size of the Jacobian matrix grows quadratically with the number of species in the model. We conclude that the simulation scheme presented in this paper provides a reliable and efficient tool for simulation of the population dynamics of sinking phytoplankton species in light-limited environments.

From a biological perspective, our results support the earlier finding that Sverdrup's critical-depth theory [38] does not hold if the turbulent mixing rate is reduced below a critical threshold level (see also [20, 21, 11]). Instead, there exists a 'turbulence window' for the persistence of sinking phytoplankton species in unstratified waters [18]. If turbulent diffusion is high, Sverdrup's theory applies and, accordingly, in deep waters the depth-averaged light conditions experienced by the phytoplankton may become too low to allow net phytoplankton growth. Conversely, if turbulent diffusion is low, sinking phytoplankton species may tumble downwards and are lost in the dark. At intermediate levels of turbulence, however, phytoplankton growth rates in the euphotic zone may exceed both mixing rates and sinking rates. As a result, at intermediate turbulence levels, populations of sinking phytoplankton can be sustained even if all individuals within the population have a tendency to sink.

The turbulence window for stratified waters is similar to the turbulence window in unstratified waters (compare Fig. 3 and Fig. 5). Additionally, the growth of sinking phytoplankton in stratified waters is restricted by a minimal thermocline depth. That is, if the thermocline in a stratified water column shallows, then export of sinking phytoplankton over the thermocline may become too high, and the phytoplankton population cannot be prevented from sinking downwards. Experiments and field observations confirm the existence of such a minimal thermocline depth for sinking phytoplankton [32, 40, 7, 9].

Summarizing, our results show that the population dynamics of sinking phytoplankton species depend crucially on the balance between growth rates, turbulent mixing rates, and sinking rates. In some waters there will be strong selection against sinking phytoplankton species, whereas in other waters sinking species may even dominate over buoyant and neutrally buoyant phytoplankton species (Fig. 6). A proper understanding of the abundance and distribution of sinking phytoplankton species clearly requires a careful consideration of the interplay between plankton dynamics and fluid dynamics.

Acknowledgements
We thank U. Ebert for the reference to Ockham's razor, and our discussions on the topic.

References

[1] K.R. Arrigo, D.H. Robinson, D.L. Worthen, R.B. Dunbar, G.R. DiTullio, M. VanWoert, and M.P. Lizotte, *Phytoplankton community structure and the drawdown of nutrients and CO_2 in the Southern Ocean*, Science 283, 365-367 (1999).

[2] H.J.M. de Baar, J.T.M. de Jong, B.M. Löscher, C. Veth, U. Bathmann, and V. Smetacek, *Importance of iron for plankton blooms and carbon dioxide drawdown in the Southern Ocean*, Nature 373, 412-415 (1995).

[3] T. Berman and B. Shteinman, *Phytoplankton development and turbulent mixing in Lake Kinneret (1992-1996)*, Journal of Plankton Research 20, 709-726 (1998).

[4] P.W. Boyd, A.J. Watson, C.S. Law, E.R. Abraham, T. Trull, R. Murdoch, D.C.E. Bakker, A.R. Bowie, K.O. Buesseler, H. Chang, M. Charette, P. Croot, K. Downing, R. Frew, M. Gall, M. Hadfield, J. Hall, M. Harvey, G. Jameson, J. LaRoche, M. Liddicoat, R. Ling, M.T. Maldonado, R.M. McKay, S. Nodder, S. Pickmere, R. Pridmore, S. Rintoul, K. Safi, P. Sutton, R. Strzepek, K. Tanneberger, S. Turner, A. Waite, and J. Zeldis, *A mesoscale phytoplankton bloom in the polar Southern Ocean stimulated by iron fertilization*, Nature 407, 695-702 (2000).

[5] P.N. Brown, G.D. Byrne, and A.C. Hindmarsh, *VODE: a variable-coefficient ODE solver*, SIAM Journal on Scientific and Statistical Computing 10, 1038-1051 (1989).

[6] J.E. Cloern, *Tidal stirring and phytoplankton bloom dynamics in an estuary*, Journal of Marine Research 49, 203-221 (1991).

[7] S.A. Condie and M. Bormans, *The influence of density stratification on particle settling, dispersion and population growth*, Journal of Theoretical Biology 187, 65-75 (1997).

[8] W.T. De Nobel, H.C.P. Matthijs, E. von Elert, and L.R. Mur, *Comparison of the light-limited growth of the nitrogen-fixing cyanobacteria Anabaena and Aphanizomenon*, New Phytologist 138, 579-587 (1998).

[9] S. Diehl, S. Berger, R. Ptacnik, and A. Wild, *Phytoplankton, light, and nutrients in a gradient of mixing depths. II. Field experiments*, Ecology (2002) (in press).

[10] P.L. Donaghay and T.R. Osborn, *Toward a theory of biological-physical control of harmful algal bloom dynamics and impacts*, Limnology and Oceanography 42, 1283-1296 (1997).

[11] U. Ebert, M. Arrayás, N.M. Temme, B.P. Sommeijer, and J. Huisman, *Critical conditions for phytoplankton blooms*, Bulletin of Mathematical Biology 63, 1095-1124 (2001).

[12] P.G. Falkowski, R.T. Barber, and V. Smetacek, *Biogeochemical controls and feedbacks on ocean primary production*, Science 281, 200-206 (1998).

[13] P.G. Falkowski and J.A. Raven, *Aquatic Photosynthesis*, Blackwell Science, Oxford (1997).

[14] J.H. Ferziger and M. Peric, *Computational Methods for Fluid Dynamics*, 2nd ed., Springer, Berlin (1999).

[15] E. Hairer and G. Wanner, *Solving Ordinary Differential Equations II, Stiff and Differential-Algebraic Problems*, 2nd ed., Springer Series in Computational Mathematics 14, Springer Verlag, Berlin (1996).

[16] C. Hirsch, *Numerical Computation of Internal and External Flows I, Fundamentals of Numerical Discretization*, Wiley and Sons, Chichester (1988).

[17] J. Huisman, *Population dynamics of light-limited phytoplankton: microcosm experiments*, Ecology 80, 202-210 (1999).

[18] J. Huisman, M. Arrayás, U. Ebert, and B.P. Sommeijer, *How do sinking phytoplankton species manage to persist?*, American Naturalist (2002) (in press).

[19] J. Huisman, R.R. Jonker, C. Zonneveld, and F.J. Weissing, *Competition for light between phytoplankton species: experimental tests of mechanistic theory*, Ecology 80, 211-222 (1999).

[20] J. Huisman, P. van Oostveen, and F.J. Weissing, *Critical depth and critical turbulence: two different mechanisms for the development of phytoplankton blooms*, Limnology and Oceanography 44, 1781-1788 (1999).

[21] J. Huisman, P. van Oostveen, and F.J. Weissing, *Species dynamics in phytoplankton blooms: incomplete mixing and competition for light*, American Naturalist 154, 46-68 (1999).

[22] J.R. Koseff, J.K. Holen, S.G. Monismith, and J.E. Cloern, *Coupled effects of vertical mixing and benthic grazing on phytoplankton populations in shallow, turbid estuaries*, Journal of Marine Research 51, 843-868 (1993).

[23] C. Lancelot, E. Hannon, S. Bevquevort, C. Veth, and H.J.W. de Baar, *Modeling phytoplankton blooms and carbon export production in the Southern Ocean: dominant controls by light and iron in the Atlantic sector in Austral spring 1992*, Deep-Sea Research I 47, 1621-1662 (2000).

[24] M.L. Lauria, D.A. Purdie, and J. Sharples, *Contrasting phytoplankton distributions controlled by tidal turbulence in an estuary*, Journal of Marine Systems 21, 189-197 (1999).

[25] A.R. Longhurst, *Ecological Geography of the Sea*, Academic Press, San Diego (1998).

[26] L.V. Lucas, J.E. Cloern, J.R. Koseff, S.G. Monismith, and J.K. Thompson, *Does the Sverdrup critical depth model explain bloom dynamics in estuaries?*, Journal of Marine Research 56, 375-415 (1998).

[27] K.H. Mann and J.R.N. Lazier, *Dynamics of Marine Ecosystems: Biological-Physical Interactions in the Oceans*, 2nd ed., Blackwell, Oxford (1996).

[28] J.H. Martin, R.M. Gordon, and S.E. Fitzwater, *Iron in Antarctic waters*, Nature 345, 156-158 (1990).

[29] B.G. Mitchell, E.A. Brody, O. Holm-Hansen, C. McCain, and J. Bishop, *Light limitation of phytoplankton biomass and macronutrient utilization in the Southern Ocean*, Limnology and Oceanography 36, 1662-1677 (1991).

[30] J. Monod, *La technique de culture continue, théorie et applications*, Annales de l'Institut Pasteur (Paris) 79, 390-410 (1950).

[31] T. Platt, S. Sathyendranath, O. Ulloa, W.G. Harrison, N. Hoepffner, and J. Goes, *Nutrient control of phytoplankton photosynthesis in the Western North Atlantic*, Nature 356, 229-231 (1992).

[32] C.S. Reynolds, S.W. Wiseman, B.M. Godfrey, and C. Butterwick, *Some effects of artificial mixing on the dynamics of phytoplankton populations in large limnetic exclosures*, Journal of Plankton Research 5, 203-234 (1983).

[33] G.A. Riley, H. Stommel, and D.F. Bumpus, *Quantitative ecology of the plankton of the western North Atlantic*, Bulletin of the Bingham Oceanographic Collection 12, 1-169 (1949).

[34] E. Sakshaug, D. Slagstad, and O. Holm-Hansen, *Factors controlling the development of phytoplankton blooms in the Antarctic Ocean: a mathematical model*, Marine Chemistry 35, 259-271 (1991).

[35] J. Sharples and P. Tett, *Modelling the effect of physical variability on the midwater chlorophyll maximum*, Journal of Marine Research 52, 219-238 (1994).

[36] B.S. Sherman, I.T. Webster, G.J. Jones, and R.L. Oliver, *Transitions between Aulacoseira and Anabaena dominance in a turbid river weir pool*, Limnology and Oceanography 43, 1902-1915 (1998).

[37] W.G. Sunda and S.A. Huntsman, *Interrelated influence of iron, light and cell size on marine phytoplankton growth*, Nature 390, 389-392 (1997).

[38] H.U. Sverdrup, *On conditions for the vernal blooming of phytoplankton*, Journal du Conseil Permanent International pour l'Exploration de la Mer 18, 287-295 (1953).

[39] P.M. Visser, B.W. Ibelings, B. van der Veer, J. Koedood, and L.R. Mur, *Artificial mixing prevents nuisance blooms of the cyanobacterium Microcystis in Lake Nieuwe Meer, The Netherlands*, Freshwater Biology 36, 435-450 (1996).

[40] P.M. Visser, L. Massaut, J. Huisman, and L.R. Mur, *Sedimentation losses of Scenedesmus in relation to mixing depth*, Archiv für Hydrobiologie 136, 289-308 (1996).

[41] P.M. Visser, J. Passarge, and L.R. Mur, *Modelling vertical migration of the cyanobacterium Microcystis*, Hydrobiologia 349, 99-109 (1997).

[42] A.J. Watson, D.C.E. Bakker, A.J. Ridgwell, P.W. Boyd, and C.S. Law, *Effect of iron supply on Southern Ocean CO_2 uptake and implications for glacial atmospheric CO_2*, Nature 407, 730-733 (2000).